

Article

Example-based Multispectral Photometric Stereo for Multi-colored surfaces

Daisuke Miyazaki^{1*}  and Kazuya Uegomori¹

¹ Graduate School of Information Sciences, Hiroshima City University, Hiroshima 731-3194, Japan

* Correspondence: miyazaki@hiroshima-cu.ac.jp

Version June 22, 2022 submitted to J. Imaging

Abstract: Photometric stereo needs three images taken under three different light directions lit one by one, while color photometric stereo needs only one image taken under three different lights lit at the same time with different light directions and different colors. As a result, color photometric stereo can obtain the surface normal of dynamically moving object from a single image. However, the conventional color photometric stereo cannot estimate a multicolored object due to the colored illumination. This paper use example-based photometric stereo for solving the problem of color photometric stereo. Example-based photometric stereo searches the surface normal from the database of the images of known shapes. Color photometric stereos suffer from mathematical difficulty, and they add many assumptions and constraints, however, example-based photometric stereo is free from such mathematical problems. The process of our method is pixelwise, thus, the estimated surface normal is not oversmoothed, unlike existing methods that use smoothness constraints. To demonstrate the effectiveness of this study, a measurement device that can realize the multispectral photometric stereo method with 16 colors is employed instead of the classic color photometric stereo method with 3 colors.

Keywords: photometric stereo; color photometric stereo; example-based photometric stereo; multispectral imaging; multispectral lighting

1. Introduction

The photometric stereo method is not suitable for modeling a moving object since several images by changing the direction of the light source are needed. The color photometric stereo method can measure the shape of a moving object, which employs red, green, and blue lights in three different directions. Unlike the common color photometric stereo method, we use 16 narrow-band lights with different peak wavelengths while observing the target object with a 16-band multispectral camera.

1.1. Related work

The shape-from-shading method [1–6] and the photometric stereo method [7,8] estimates the surface normal of an object by illuminating the object and analyzing the resulting shadings on the object's surface. Unlike shape-from-shading which uses one image, photometric stereo captures three images with different light source directions. Therefore, it is impossible to measure a dynamic object. This problem can be resolved using the color photometric stereo method [9–28] (also known as shape-from-color). Color photometric stereo takes one picture with an RGB color camera under red, green, and blue light sources. Such a one-shot photograph enables the measurement of a dynamic object. However, the color photometric stereo has many problems. The major problem of the color photometric stereo method is the fact that it can only be used with white objects. This is an inevitable problem as long as lights are illuminated from colored light sources to estimate the surface normal.

34 Some methods [20,25,29] use multiple images to apply color photometric stereo to multicolored
35 objects. These methods cannot estimate the surface normal from a single image, thus, the optical
36 flow method is used to track the identical point on the object surface among multiple images. Fyffe
37 et al. [16] used three lights that can be recognized as white color by the human eye. The target
38 objects are observed by six band camera. Each three light has different spectral distribution, which
39 can be distinguished by the six band camera. They estimate the surface normal without disturbing
40 the human eye's appearance. As done by Anderson et al. [9], using the shape from other methods
41 such as multiview stereo enables the color photometric stereo to be applied to multicolored objects.
42 Chakrabarti et al. [11] and Jiao et al. [19] assumed that a certain limited area has the same albedo.
43 This assumption enables color photometric stereo to be applied to multicolored objects which can be
44 segmented for each colored region.

45 Example-based photometric stereos [30–34] estimate the surface normal using a database search.
46 Those methods capture some images of objects with known shapes. They assume that the material
47 properties of the objects in the database and the objects to be measured are the same. If the
48 appearances of the pixels among those two types of objects are the same, these pixels might have the
49 same surface normal. The example-based photometric stereo is used for a conventional photometric
50 stereo problem which assumes the same albedo for each light and is not used for the color photometric
51 stereo problem since the albedo differs for each light.

52 1.2. Our work

53 In this paper, the problem faced by the color photometric stereo method is solved using a
54 different approach from those used in previous studies. We use the example-based photometric stereo
55 to solve the problem of the color photometric stereo. Our approach solves the problem of shadow,
56 specular reflection, and channel crosstalk.

57 Unlike Guo et al. [35], our method can be applied to the objects whose chromaticity and albedo
58 are both spatially varying. The techniques of Gotardo et al. [29], Kim et al. [20], and Roubtsova
59 et al. [25] need to employ optical flow to measure a dynamic object, while the technique of Fyffe
60 et al. [16] requires a reflectance database to be prepared prior to the measurement. Our proposed
61 technique does not require a shape obtained from other sensors such as multi-view stereo or laser
62 sensor, unlike the technique of Anderson et al. [9] Moreover, unlike the techniques of Chakrabarti et
63 al. [11] and Jiao et al., [19] our proposed method does not require region segmentation. Our method
64 is not oversmoothed by median filtering [36] and is not affected by randomness [37].

65 Previous color photometric stereo methods used three lights with red, green, and blue colors and
66 observed the object with an RGB color camera. In our study, 16 lights with different wavelengths are
67 used to illuminate the object, which is then observed by a 16-band multispectral camera. This paper
68 empirically proves that the example-based photometric stereo is also useful for the color photometric
69 stereo situations.

70 Section 2 and 3 explain the fundamental theory of color photometric stereo and example-based
71 photometric stereo, respectively. Section 4 explains our example-based multispectral photometric
72 stereo. Especially, Section 5.5 discusses the advantages and disadvantages of our method. Section 5
73 and 6 show the experimental results and the conclusion, respectively.

74 2. Color photometric stereo

75 A photometric stereo method that employs independent colored light is called the color
76 photometric stereo method. A characteristic of this method is that it enables the estimation of the
77 surface normal with one photoshoot. The widespread color photometric stereo method is conducted
78 with three types of colored lights. While the conventional photometric stereo method results in
79 several grayscale images, the color photometric stereo method results in a multi-spectral image.

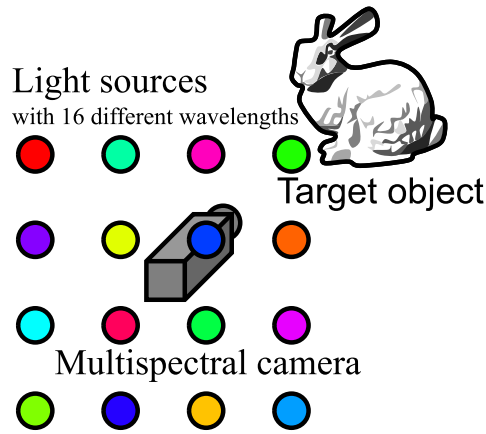


Figure 1. Conceptual explanation of multispectral color photometric stereo. Target object is illuminated by multiple light sources whose wavelengths are different. One image is taken using multispectral camera.

Given \mathbf{n} as a normal vector and \mathbf{l}_c as the light source direction vector of channel c , then the multispectral image can be:

$$I_c = A_c \max(\mathbf{n} \cdot \mathbf{l}_c, 0) \quad . \quad (1)$$

80 Hereinafter, we call A_c albedo. Note that the camera sensitivity and light source brightness are
81 included in A_c .

82 As shown in Fig. 1, this study conducts a photoshoot of a multicolored object using 16 channels.
83 Following Eq. (1), the brightness is obtained from this photoshoot as follows.

$$\begin{aligned} I_0 &= A_0 \max(\mathbf{n} \cdot \mathbf{l}_0, 0), \\ I_1 &= A_1 \max(\mathbf{n} \cdot \mathbf{l}_1, 0), \\ &\vdots \\ I_{15} &= A_{15} \max(\mathbf{n} \cdot \mathbf{l}_{15}, 0). \end{aligned} \quad (2)$$

84 The surface normal \mathbf{n} is a 3D vector; however, the degree-of-freedom is two because it is
85 constrained to be a unit vector (such constraint reduces one degree-of-freedom). Albedo A_c is
86 represented by 16 parameters. There are 16 equations, as shown in Eq. (2), and 18 unknown
87 parameters ($A_0, A_1, \dots, A_{15}, n_x, n_y, n_z$, s.t., $n_x^2 + n_y^2 + n_z^2 = 1$, namely 16 for albedo and 2 for surface
88 normal). Therefore, color photometric stereo is an ill-posed problem.

89 The most commonly used assumption is to limit the color of the target objects to white
90 ($A_0 = A_1 = \dots = A_{15}$). The color photometric stereo for white objects, or in other words, the
91 conventional photometric stereo can directly solve the surface normal, without iterative optimization
92 nor additional constraints such as smoothness constraints. However, this paper analyzes the methods
93 with multi-colored objects.

94 3. Example-based photometric stereo

95 Example-based photometric stereo (Fig. 2) uses the reference objects with known shapes for
96 estimating surface normal which can be applied to non-Lambertian surfaces. Example-based
97 photometric stereo measures two objects with known and unknown shapes under the same scene.
98 Those two objects should have the same material property.

99 A sphere is often used for reference objects. Both brightnesses coincide if the surface normal of
100 the target object and the surface normal of the reference object coincide because the material property,
101 light direction, and camera direction are the same. Therefore, example-based photometric stereo can

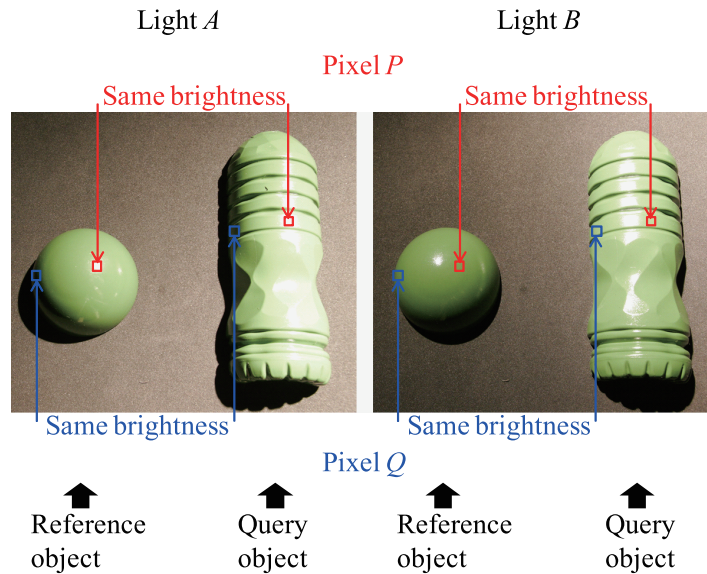


Figure 2. Brightness search of example-based photometric stereo.

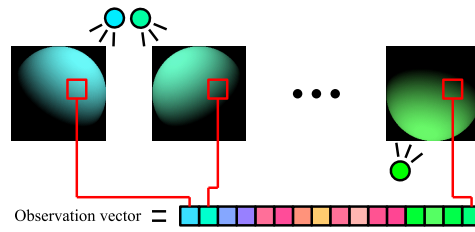


Figure 3. Observation vector.

102 estimate the surface normal of the objects with an arbitrary BRDF (bidirectional reflection distribution
 103 function). The disadvantage of example-based photometric stereo is that the reference objects whose
 104 material property is the same as the target objects are needed. The interreflection between each
 105 surface point is not considered in this method.

106 4. Proposed method

107 4.1. Example-based multispectral photometric stereo

108 Existing methods add some constraints such as smoothness to solve since the unknowns exceed
 109 the inputs. Such an approach oversmooths the albedo and the surface normal. Our method does not
 110 require any constraints.

111 We observe the object illuminated under 16 lights with different wavelengths by the
 112 multispectral camera (Fig. 1). The observation vector at pixel (y_Q, x_Q) of query image (the image
 113 of target object) is denoted as $(I_{Q,0}, I_{Q,1}, \dots, I_{Q,15})^\top$ and the observation vector at pixel (y_R, x_R)
 114 of reference image (the image of the database) is denoted as $(I_{R,0}, I_{R,1}, \dots, I_{R,15})^\top$. If query's
 115 albedo $(A_{Q,0}, A_{Q,1}, \dots, A_{Q,15})^\top$ and reference's albedo $(A_{R,0}, A_{R,1}, \dots, A_{R,15})^\top$ coincide and query's
 116 observation vector and reference's observation vector coincide, the surface normal at (y_R, x_R) and the
 117 surface normal at (y_Q, x_Q) coincide. Each element of the 16-dimensional observation vector (Fig. 3) is
 118 Eq. (2).

119 We search the pixel position of the reference object where the query's observation vector
 120 coincides with the reference's observation vector (Fig. 4). The query's surface normal is determined

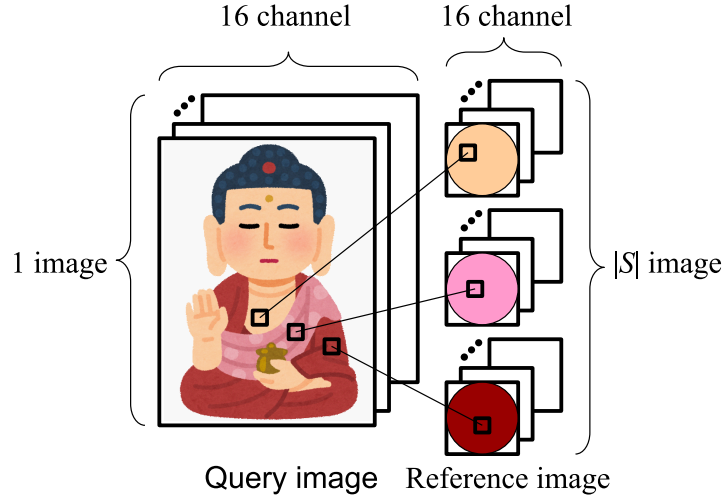


Figure 4. Our approach.

121 from the pixel position of the reference found. Multiple spheres with different paints are used as the
 122 reference. The search of the observation vector is performed for all pixels of all reference spheres.

123 Our method (Eq. (3)) searches the pixel position where the squared error of 16-dimensional
 124 vector becomes the minimum.

$$\begin{aligned} \mathbf{n}(y_Q, x_Q) &= \mathbf{n}_R(y_R, x_R), \\ \text{s.t. } (y_R, x_R) &= \underset{y_R, x_R}{\operatorname{argmin}} \sum_{c \in \mathcal{C}} (I_Q(y_Q, x_Q, c) - I_R(s, y_R, x_R, c))^2, \quad \forall s \in \mathcal{S}, \quad \forall (y_R, x_R) \in \mathcal{P}_R. \end{aligned} \quad (3)$$

125 Here, $|\mathcal{C}|$ is the number of channels ($|\mathcal{C}| = 16$), $|\mathcal{S}|$ is the number of reference objects, and \mathcal{P}_R
 126 is a set of reference's pixels. We normalize the observation vectors of both the query image and the
 127 reference image. Thanks to the normalization, our method can be applied even if the camera exposure
 128 is changed.

129 In order to apply our method to any objects with any paints, we have to measure all paints in
 130 the world. However, the variation of paints is limited due to the limitation of chemical reactions.
 131 The number of paints is limited if the paints are based on pure natural pigments since the number
 132 of natural pigments is limited. In this paper, we assume that all paints can be expressed in a limited
 133 number. We used 18 spheres with different color ($|\mathcal{S}| = 18$).

134 4.2. Converting surface normal to height

The shape is represented as the height H set for each pixel. The partial derivatives of the heights
 with respect to x and y are called gradient, and represented as p and q , respectively.

$$p = H_x = \frac{\partial H}{\partial x}, \quad q = H_y = \frac{\partial H}{\partial y}. \quad (4)$$

The surface normal \mathbf{n} is represented by these gradients as shown below.

$$\mathbf{n} = \frac{(-p, -q, 1)^T}{\sqrt{p^2 + q^2 + 1}}. \quad (5)$$

The cost function that relates the surface normal to the height is shown below.

$$\iint (H_x - p)^2 + (H_y - q)^2 dx dy. \quad (6)$$

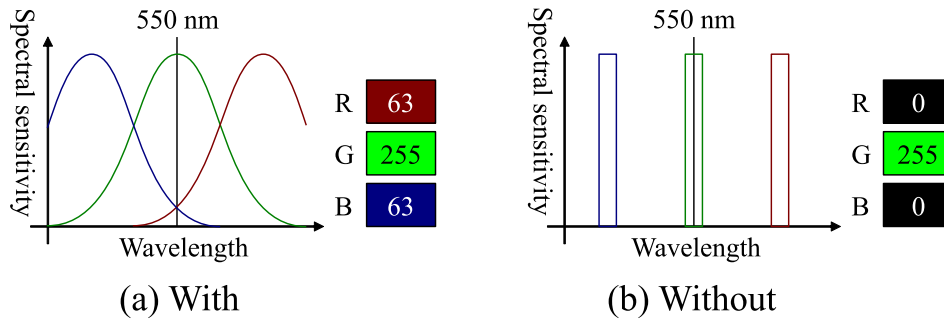


Figure 5. Example of camera spectral sensitivity: (a) The sensor which has channel crosstalk and (b) the sensor which does not have channel crosstalk.

135 We solve Eq. (6) to calculate the height from the surface normal, using existing techniques.

136 4.3. Channel crosstalk

137 Conventional color photometric stereo assumes that the camera spectral response is a delta
 138 function. Fig. 5 (b) is an example where only the G channel detects the 550 [nm] light. On the
 139 other hand, Fig. 5 (a) is an example where the sensor has channel crosstalks. Namely, the spectral
 140 responses of R, G, and B channels partially overlap in the spectral domain. In this example, the sensor
 141 detects $(R, G, B) = (63, 255, 63)$ instead of $(R, G, B) = (0, 255, 0)$ (Fig. 5 (b)) when 550 [nm] light is
 142 observed. Namely, the red and blue channels are excited even if the observed light is completely
 143 green. Such channel crosstalk is annoying for conventional color photometric stereo. Conventional
 144 color photometric stereo assumes that, for example, only the green channel should detect the green
 145 light. Channel crosstalk commonly occurs in most cameras, which makes the color photometric stereo
 146 difficult. However, as discussed in Section 5.5, our method is free from the channel crosstalk problem.

147 5. Experiment

148 5.1. Experimental setup

149 We perform our experiment in a dark room as shown in Fig. 6 where the target object is
 150 illuminated under 16 different lights. We use IMEC-HS-16-USB-customized (Imec, Belgium) for the
 151 multispectral camera. Fig. 7 and Table 1 show the spectral sensitivity of the camera, where channel
 152 crosstalks are occurring among all camera channels. Table 2 shows the peak wavelength for each light
 153 source used in this experiment. To increase the amount of supplementary information obtained for
 154 objects with narrow-wavelength regions, light sources of close wavelength were positioned opposite
 155 to each other. Namely, as shown in Table 2, the light of the next larger wavelength is set far apart in
 156 more than one Manhattan distance in 4×4 grid. The locations of the light sources and the camera
 157 were left unchanged during the experiments. We assume that the light source and the camera are
 158 infinite far from the target object. This paper represents the surface normal as pseudo-color where x ,
 159 y , and z of the normal vector is mapped to R, G, and B of the image. Each sphere image is trimmed
 160 and scaled to 128×128 size. The sphere objects shown in Fig. 8 are painted with 18 different paints.
 161 The size of the query image is 512×256 . The target object is opaque objects. Our method can estimate
 162 the surface normal of metals if the number of lights is infinity, while it cannot estimate due to the finite
 163 number of lights. Transparent objects are more difficult to measure due to the transmission.

164 5.2. Evaluation

165 First, we measured a spherical object, shown in Fig. 9 (a), consisting of two types of albedos
 166 painted with the paints included in the reference objects. The error is evaluated as an angle between
 167 the estimated surface normal and the true surface normal. We have to compare the estimated surface

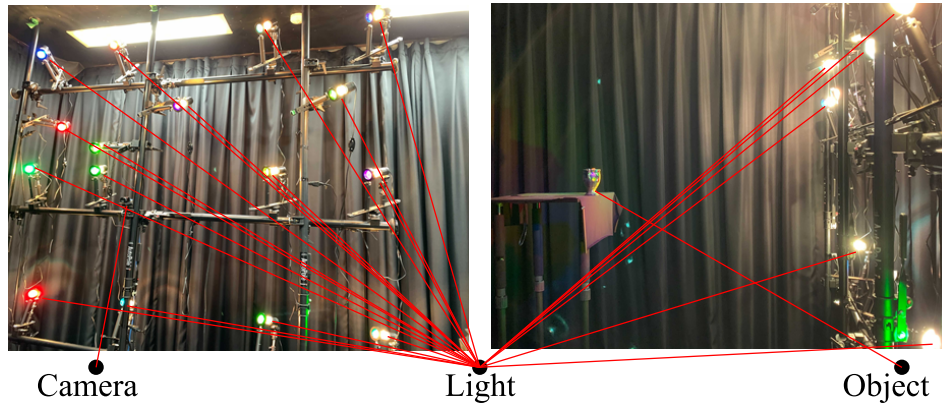


Figure 6. Experimental apparatus.

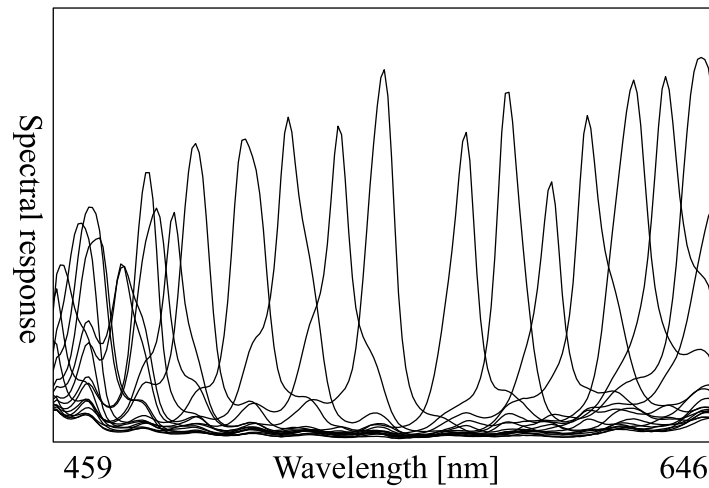


Figure 7. Spectral response of the camera.

Table 1. The spectral response for each channel of the camera.

Channel 1 Peak 488 nm Peak 50% 488–492 nm	Channel 2 Peak 499 nm Peak 50% 495–503 nm	Channel 3 Peak 479 nm Peak 50% 467–486 nm	Channel 4 Peak 469 nm Peak 50% 464–474 nm
Channel 5 Peak 599 nm Peak 50% 459–465, 595–602 nm	Channel 6 Peak 609 nm Peak 50% 464–470, 606–615 nm	Channel 7 Peak 587 nm Peak 50% 583–591 nm	Channel 8 Peak 575 nm Peak 50% 570–578 nm
Channel 9 Peak 641 nm Peak 50% 483–488, 635–646 nm	Channel 10 Peak 644 nm Peak 50% 489–497, 637–646 nm	Channel 11 Peak 631 nm Peak 50% 626–638 nm	Channel 12 Peak 622 nm Peak 50% 468–473, 616–627 nm
Channel 13 Peak 539 nm Peak 50% 535–543 nm	Channel 14 Peak 552 nm Peak 50% 547–555 nm	Channel 15 Peak 525 nm Peak 50% 521–532 nm	Channel 16 Peak 513 nm Peak 50% 509–519 nm

Table 2. Peak wavelength of each light (10nm width).

Light 1 488 nm	Light 2 632 nm	Light 3 540 nm	Light 4 500 nm
Light 5 647 nm	Light 6 600 nm	Light 7 470 nm	Light 8 610 nm
Light 9 520 nm	Light 10 568 nm	Light 11 620 nm	Light 12 473 nm
Light 13 636 nm	Light 14 515 nm	Light 15 589 nm	Light 16 550 nm

**Figure 8.** Reference objects.

168 normal with the true surface normal by measuring the object whose true surface normal is known.
 169 We measured a sphere for evaluation. The mathematically true surface normal can be theoretically
 170 derived from the sphere's center and radius. Suppose that the pixel of interest is (x, y) and the center
 171 of the sphere is (\bar{x}, \bar{y}) . Suppose that the radius of the sphere is r . Then, the true surface normal
 172 (n_x, n_y, n_z) can be calculated as follows:

$$n_x = (x - \bar{x}) / r, \quad (7)$$

$$n_y = -(y - \bar{y}) / r, \quad (8)$$

$$n_z = \sqrt{1 - n_x^2 - n_y^2}. \quad (9)$$

173 Since we know the true surface normal from Eq. (7)–(9), we can evaluate the performance of the
 174 method by measuring a sphere. Fig. 9 (b), (c), and (d) show the error map with pseudo-color
 175 representation. We compared our method with the conventional photometric stereo (Fig. 9 (b)).
 176 The color photometric stereo that assumes white objects as targets is the same as the conventional
 177 photometric stereo. Also, we compared our method with existing method [35] (Fig. 9 (c)). The error
 178 of conventional photometric stereo (color photometric stereo with white object) was 0.690 [rad], the
 179 error of existing method (Guo et al. [35]) was 0.888 [rad], and the error of our method was 0.198 [rad],
 180 which proves the high performances of our method.

181 5.3. Real objects

182 We apply the existing method [36] and our method to the object shown in Fig. 10 (a). The
 183 estimated surface normals of existing and our methods are shown in Fig. 10 (b) and (c), respectively.
 184 Here, the surface normal of x , y , and z axes are represented as red, green, and blue color. Unlike the
 185 existing method which oversmooths the result (Fig. 10 (b)), our method is a pixelwise approach, and
 186 the result is not oversmoothed (Fig. 10 (c)). Existing method [36] needs to segment the object region
 187 from the background (Fig. 10 (b)), while our method do not need to distinguish the foreground and

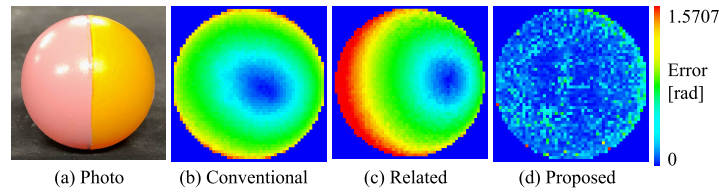


Figure 9. Performance evaluation result: (a) Target spherical object with 2 paints, (b) the error map of conventional photometric stereo, (c) the error map of existing method, and (d) the error map of proposed method.

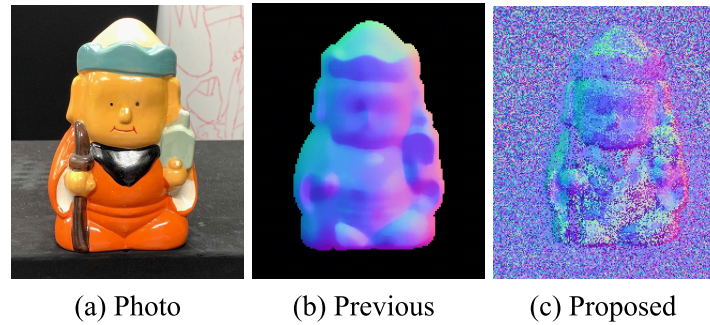


Figure 10. Comparison: (a) Target object, (b) the estimated surface normal of previous method, and (c) the estimated surface normal of proposed method.

188 the background. Existing method cannot estimate the surface normal of the background while our
 189 method can, however, the surface normal of the background is just a noise since the background has
 190 no object with completely dark void with random noise (Fig. 10 (c)).

191 The target objects are shown in Fig. 11 (a). The paints used in Fig. 11 (3)–(4) are included in
 192 the reference data, while the others are not. The results of a multi-colored object, a white object,
 193 a single-colored object, an object with dark color, and a deformable object with two different pose
 194 are shown in Fig. 11 (1)–(6), respectively. The estimated surface normals of our method are shown
 195 in Fig. 11 (b). Fig. 11 (c) and Fig. 11 (d) show the reconstructed shapes under two different viewing
 196 directions. The quantitative evaluation shown in Section 5.2 proves the benefit of our method, and the
 197 qualitative evaluation shown in Fig. 11 also proves the benefit of our method. As shown in Fig. 11, our
 198 method can successfully estimate the surface normals for both achromatic (Fig. 11 (2)) and chromatic
 199 (Fig. 11 (1)) objects without oversmoothing them.

200 5.4. Discussion

201 We dare not to add smoothness constraints, and thus, our result is not oversmoothed. Adding
 202 smoothness constraint results in smoother results which are often required by the users. If we
 203 add some constraints, we have to tune the parameters of those constraints. Fig. 12 shows the
 204 parameter tuning problem that occurred in the existing method [36]. One of our future work is to add
 205 smoothness constraints, but we have to carefully design the algorithm because adding smoothness
 206 constraints is not always a good approach due to the oversmoothing and parameter tuning.

207 Our method is applicable to multi-colored objects as shown in the experiments where error did
 208 not occur at the color boundary of the object (Fig. 11 (1)). Our method is robust to specular reflection
 209 as shown in the experiments that the spike-like error has not appeared in the result (Fig. 9 (c)). Our
 210 method cannot estimate the surface normal of the dark surface, however, this disadvantage is always
 211 true to all other photometric stereo methods (Fig. 11 (4)).

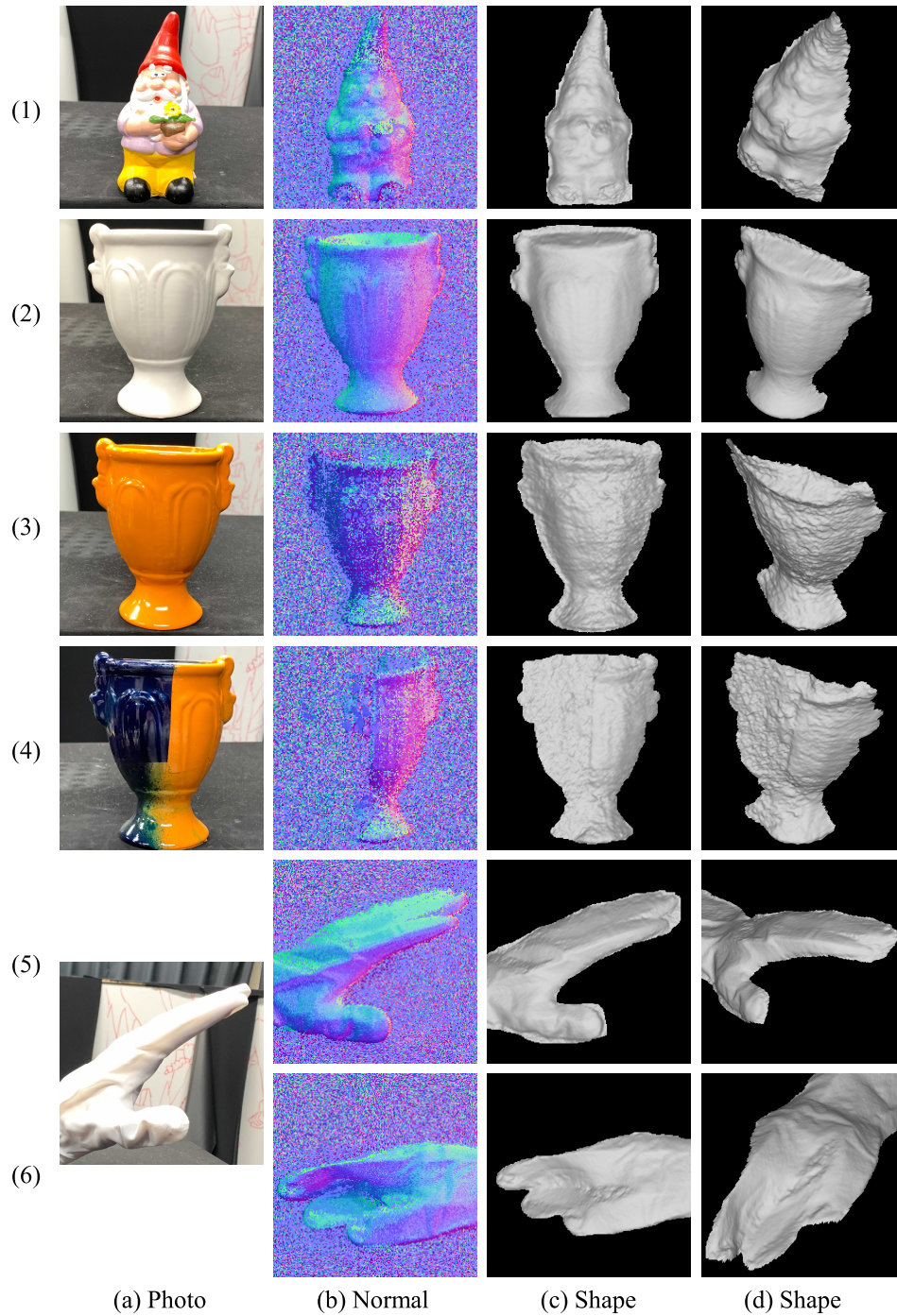


Figure 11. Experimental result of (1) multi-colored object, (2) white object, (3) single-colored object, (4) dark object, and (5)(6) deformable object: (a) Target object, (b) estimated surface normal, and (c)(d) reconstructed shape.

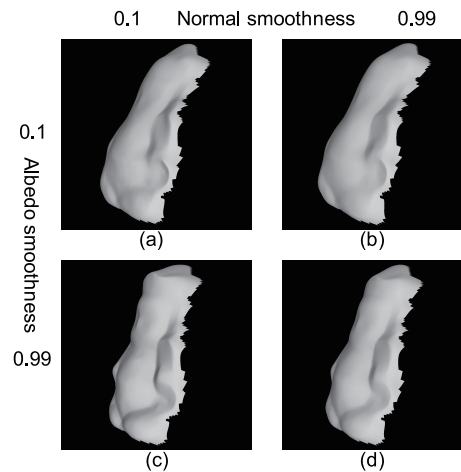


Figure 12. Parameter tuning problem of previous method: (a) Sharp normal and sharp albedo, (b) smooth normal and sharp albedo, (c) sharp normal and smooth albedo, and (d) smooth normal and smooth albedo.

212 5.5. Contribution

213 Here, we summarize our advantage and disadvantage.

214 Our method does not suffer from channel crosstalk, since the reference object includes the
 215 information of channel crosstalk, and the query object and the reference object are measured under
 216 the same light and the same camera. Namely, our method is not affected by the spectral distribution
 217 of the lights and the spectral/radiometric response of the camera, since both query and reference
 218 objects are measured under the same lights and with the same camera. Our process is pixelwise,
 219 and thus, the result is not affected by neighboring pixels. The light source direction is not needed to
 220 be measured, because the target and reference objects are illuminated under the same illumination
 221 environment. Also, we do not adjust each light source to be the same intensity. Our method is not
 222 limited to a Lambertian surface, and our method is not affected by shadows. If we prepare reference
 223 objects with specular reflection, our method can be applied to the objects with specular reflection.

224 The disadvantage of our method is that we need many reference objects. Also, we have to
 225 measure the query object with the same device that the reference objects are taken, since the light
 226 and the camera information are included in the reference objects.

227 The number of reference objects is related to both advantages and disadvantages. If we
 228 increase reference objects, our method can be applied to various types of paints. However, a
 229 similar observation vector might appear in the database if we increase reference objects. These are
 230 the characteristics of example-based multispectral photometric stereo compared to example-based
 231 conventional photometric stereo. The albedo A_0, A_1, \dots, A_{15} has 16 degree-of-freedom in our
 232 method but has 1 degree-of-freedom in example-based photometric stereo. Due to the wider
 233 degree-of-freedom, the unique database search is disabled if we use many reference objects. This is
 234 the dilemma of our method whether we should increase or decrease the number of reference objects.

235 6. Conclusion

236 Our method estimated the surface normal of multi-colored objects using 16 lights. The light
 237 source directions of all lights are not needed to be measured. The query and reference objects
 238 are observed by a multispectral camera. We measured many spheres painted with a single color
 239 with various paints. Surface normals are the same for the two points on the surface if the material
 240 properties are the same, the light source directions are the same, and the camera direction is the same.

241 We estimated the surface normal of the target object by finding the pixel where the data of the query
242 image becomes the same as the data of the reference images.

243 Our experimental results show that our method has successfully estimated the surface normal
244 of multi-colored objects. However, the dark albedo has caused some amount of error.

245 This time, we scanned all reference objects. However, it is well known that the spectral
246 reflectance of any paint can be represented with a small number of basis functions. We conjecture
247 that the bases of the PCA (principal component analysis) can represent the data with a small number
248 of basis functions. Our future work is to install PCA in our method.

249 **Author Contributions:** Conceptualization, D.M.; methodology, D.M.; software, D.M. and K.U.; validation, D.M.
250 and K.U.; formal analysis, D.M. and K.U.; investigation, D.M.; resources, D.M.; data curation, D.M. and K.U.;
251 writing—original draft preparation, D.M. and K.U.; writing—review and editing, D.M.; visualization, D.M. and
252 K.U.; supervision, D.M.; project administration, D.M.; funding acquisition, D.M.

253 **Funding:** This research was supported in part by JSPS KAKENHI Grant Number 18H04119, and in part by JSPS
254 KAKENHI Grant Number 20H00612.

255 **Institutional Review Board Statement:** Not applicable.

256 **Informed Consent Statement:** Not applicable.

257 **Data Availability Statement:** Not applicable.

258 **Acknowledgments:** The authors thank Ryo Furukawa, Masashi Baba, and Michihiro Mikamo for useful
259 discussions.

260 **Conflicts of Interest:** The authors declare no conflict of interest.

261 References

- 262 1. T. Rindfleisch, "Photometric method for lunar topography," *Photogrammetric Engineering*, vol. 32, no. 2,
263 pp. 262–277, 1966.
- 264 2. B. K. P. Horn, "Obtaining shape from shading information," in *The Psychology of Computer Vision*, P. H.
265 Winston (Ed.), McGraw-Hill, New York, pp. 115–155, 1975.
- 266 3. B. K. P. Horn and M. J. Brooks, "The variational approach to shape from shading," *Computer Vision, Graphics,*
267 *and Image Processing*, vol. 33, no. 2, pp. 174–208, 1986.
- 268 4. B. K. P. Horn, "Height and gradient from shading," *International Journal of Computer Vision*, vol. 5, pp. 37–75,
269 1990.
- 270 5. R. Zhang, P. S. Tsai, J. E. Cryer, and M. Shah, "Shape-from-shading: a survey," *IEEE Transactions on Pattern*
271 *Analysis and Machine Intelligence*, vol. 21, no. 8, pp. 690–706, 1999.
- 272 6. J.-D. Durou, M. Falcone, and M. Sagona, "Numerical methods for shape-from-shading: a new survey with
273 benchmarks", *Computer Vision and Image Understanding*, vol. 109, no. 1, pp. 22–43, 2008.
- 274 7. W. M. Silver, "Determining shape and reflectance using multiple images," *Master's thesis*, Massachusetts
275 Institute of Technology, 1980.
- 276 8. R. J. Woodham, "Photometric method for determining surface orientation from multiple images," *Optical*
277 *Engineering*, vol. 19, no. 1, pp. 139–144, 1980.
- 278 9. R. Anderson, B. Stenger, and R. Cipolla, "Color photometric stereo for multicolored surfaces," In
279 *International Conference on Computer Vision*, pp. 2182–2189, 2011.
- 280 10. G. J. Brostow, B. Stenger, G. Vogiatzis, C. Hernández, and R. Cipolla, "Video normals from colored lights,"
281 *IEEE Transactions on Pattern Analysis and Machine Intelligence*, vol. 33, no. 10, pp. 2104–2114, 2011.
- 282 11. A. Chakrabarti and K. Sunkavalli, "Single-image RGB photometric stereo with spatially-varying albedo,"
283 In *International Conference on 3D Vision*, pp. 258–266, 2016.
- 284 12. M. Drew and L. Kontsevich, "Closed-form attitude determination under spectrally varying illumination,"
285 In *IEEE Conference on Computer Vision and Pattern Recognition*, pp. 985–990, 1994.
- 286 13. M. S. Drew, "Reduction of rank-reduced orientation-from-color problem with many unknown lights to
287 two-image known-illuminant photometric stereo," In *Proceedings of International Symposium on Computer*
288 *Vision*, pp. 419–424, 1995.

- 289 14. M. S. Drew, "Direct solution of orientation-from-color problem using a modification of Pentland's light
290 source direction estimator," *Computer Vision and Image Understanding*, vol. 64, no. 2, pp. 286–299, 1996.
- 291 15. M. S. Drew and M. H. Brill, "Color from shape from color: a simple formalism with known light sources,"
292 *Journal of the Optical Society of America A*, vol. 17, no. 8, pp. 1371–1381, 2000.
- 293 16. G. Fyffe, X. Yu, and P. Debevec, "Single-shot photometric stereo by spectral multiplexing," *IEEE*
294 *International Conference on Computational Photography*, pp. 1–6, 2011.
- 295 17. C. Hernandez, G. Vogiatzis, G. J. Brostow, B. Stenger, and R. Cipolla, "Non-rigid photometric stereo with
296 colored lights," In *IEEE International Conference on Computer Vision*, pp. 8, 2007.
- 297 18. C. Hernández, G. Vogiatzis, and R. Cipolla, "Shadows in three-source photometric stereo," In *European*
298 *Conference on Computer Vision*; Springer: Berlin/Heidelberg, Germany, 2008; pp. 290–303.
- 299 19. H. Jiao, Y. Luo, N. Wang, L. Qi, J. Dong, and H. Lei, "Underwater multi-spectral photometric stereo
300 reconstruction from a single RGBD image," In *Asia-Pacific Signal and Information Processing Association*
301 *Annual Summit and Conference*, pp. 1–4, 2016.
- 302 20. H. Kim, B. Wilburn, and M. Ben-Ezra, "Photometric stereo for dynamic surface orientations," In *European*
303 *Conference on Computer Vision*, LNCS 6311, pp. 59–72, 2010.
- 304 21. L. Kontsevich, A. Petrov, and I. Vergelskaya, "Reconstruction of shape from shading in color images,"
305 *Journal of Optical Society of America A*, vol. 11, pp. 1047–1052, 1994.
- 306 22. A. Landstrom, M. J. Thurley, and H. Jonsson, "Sub-millimeter crack detection in casted steel using color
307 photometric stereo," In *International Conference on Digital Image Computing: Techniques and Applications*,
308 pp. 1–7, 2013.
- 309 23. A. P. Petrov and L. L. Kontsevich, "Properties of color images of surfaces under multiple illuminants," *J.*
310 *Opt. Soc. Am. A*, vol. 11, no. 10, pp. 2745–2749, 1994.
- 311 24. S. Rahman, A. Lam, I. Sato, and A. Robles-Kelly, "Color photometric stereo using a rainbow light for
312 non-Lambertian multicolored surfaces," In *Asian Conference on Computer Vision*, pp. 335–350, 2015.
- 313 25. N. Roubtsova and J. Y. Guillemaut, "Colour Helmholtz stereopsis for reconstruction of complex dynamic
314 scenes," In *International Conference on 3D Vision*, pp. 251–258, 2014.
- 315 26. G. Vogiatzis and C. Hernández, "Practical 3d reconstruction based on photometric stereo," pp. 313–345. In:
316 R. Cipolla, S. Battiato, and G. M. Farinella, "Computer Vision: Detection, Recognition and Reconstruction,"
317 *Springer Berlin Heidelberg*, Berlin, Heidelberg, 2010.
- 318 27. G. Vogiatzis and C. Hernandez, "Self-calibrated, multi-spectral photometric stereo for 3D face capture," *Int.*
319 *J. Comput. Vis.*, vol. 97, pp. 91–103, 2012.
- 320 28. R. J. Woodham, "Gradient and curvature from photometric stereo including local confidence estimation,"
321 *Journal of the Optical Society of America*, vol. 11, pp. 3050–3068, 1994.
- 322 29. P. F. U. Gotardo, T. Simon, Y. Sheikh, and I. Mathews, "Photogeometric scene flow for high-detail dynamic
323 3D reconstruction," In *IEEE International Conference on Computer Vision*, pp. 846–854, 2015.
- 324 30. D. B. Goldman, B. Curless, A. Hertzmann, and S. M. Seitz, "Shape and spatially-varying BRDFs
325 from photometric stereo," *IEEE Transactions on Pattern Analysis and Machine Intelligence*, vol. 32, no. 6,
326 pp. 1060–1071, 2010.
- 327 31. A. Hertzmann and S. M. Seitz, "Example-based photometric stereo: shape reconstruction with general,
328 varying BRDFs," *IEEE Transactions on Pattern Analysis and Machine Intelligence*, vol. 27, no. 8, pp. 1254–1264,
329 2005.
- 330 32. B. K. P. Horn and K. Ikeuchi, "The mechanical manipulation of randomly oriented parts," *Scientific*
331 *American*, vol. 251, no. 2, pp. 100–111, 1984.
- 332 33. Z. Hui and A. C. Sankaranarayanan, "Shape and spatially-varying reflectance estimation from virtual
333 exemplars," *IEEE Transactions on Pattern Analysis and Machine Intelligence*, vol. 39, no. 10, pp. 2060–2073,
334 2017.
- 335 34. S.-K. Yeung, T.-P. Wu, C.-K. Tang, T. F. Chan, and S. Osher, "Adequate reconstruction of transparent objects
336 on a shoestring budget," In *IEEE Conference on Computer Vision and Pattern Recognition*, pp. 2513–2520, 2011.
- 337 35. H. Guo, F. Okura, B. Shi, T. Funatomi, Y. Mukaigawa, and Y. Matsushita, "Multispectral photometric stereo
338 for spatially-varying spectral reflectances: A well posed problem?," In *IEEE/CVF Conference on Computer*
339 *Vision and Pattern Recognition*, pp. 963–971, 2021.
- 340 36. D. Miyazaki, Y. Onishi, and S. Hiura, "Color photometric stereo using multi-band camera constrained by
341 median filter and occluding boundary," *Journal of Imaging*, vol. 5, no. 7, article no. 64, 29 pages, 2019.

342 37. D. Miyazaki and K. Hamaen, "Multi-band photometric stereo using random sampling of channels and
343 pixels," In *The International Workshop on Frontiers of Computer Vision*; Springer: Berlin/Heidelberg, Germany,
344 2022; pp. 79–93.

345 © 2022 by the authors. Submitted to *J. Imaging* for possible open access publication
346 under the terms and conditions of the Creative Commons Attribution (CC BY) license
347 (<http://creativecommons.org/licenses/by/4.0/>).